High-pressure lattice dynamics in wurtzite and rocksalt indium nitride investigated by means of Raman spectroscopy

J. Ibáñez,[1,*] R. Oliva,[1] F. J. Manjón,[2] A. Segura,[3] T. Yamaguchi,[4] Y. Nanishi,[4] R. Cuscó,[1] and L. Artús[1]

[1]*Institut Jaume Almera, Consell Superior d'Investigacions Científiques, 08028 Barcelona, Catalonia, Spain*

[2]*Instituto de Diseño para la Fabricación y Producción Automatizada, MALTA Consolider Team-Universitat Politècnica de València, 46022 València, Spain*

[3]*Departamento de Física Aplicada-ICMUV-MALTA Consolider Team, Universitat de València, 46100 Burjassot, València, Spain*

[4]*Faculty of Science and Engineering, Ritsumeikan University, Shiga 525-8577, Japan*

(Received 11 July 2013; published 5 September 2013)

We present an experimental and theoretical lattice-dynamical study of InN at high hydrostatic pressures. We perform Raman scattering measurements on five InN epilayers, with different residual strain and free electron concentrations. The experimental results are analyzed in terms of *ab initio* lattice-dynamical calculations on both wurtzite InN (w-InN) and rocksalt InN (rs-InN) as a function of pressure. Experimental and theoretical pressure coefficients of the optical modes in w-InN are compared, and the role of residual strain on the measured pressure coefficients is analyzed. In the case of the LO band, we analyze and discuss its pressure behavior considering the double-resonance mechanism responsible for the selective excitation of LO phonons with large wave vectors in w-InN. The pressure behavior of the L^- coupled mode observed in a heavily doped n-type sample allows us to estimate the pressure dependence of the electron effective mass in w-InN. The results thus obtained are in good agreement with $\mathbf{k} \cdot \mathbf{p}$ theory. The wurtzite-to-rocksalt phase transition on the upstroke cycle and the rocksalt-to-wurtzite backtransition on the downstroke cycle are investigated, and the Raman spectra of both phases are interpreted in terms of DFT lattice-dynamical calculations.

I. INTRODUCTION

Over the last decade, InN has attracted much research interest from both fundamental and applied points of view. The renewed attention on this compound and on the entire III-nitride alloy system was boosted after the revision of the fundamental band-gap energy of InN from 1.9 to 0.65 eV, extending the expected emission range of III-nitride alloys from deep-UV (AlN) down to the near-IR region (InN).[1,2] InN also exhibits unique transport properties, such as a small electron effective mass, a surface accumulation layer with ultra-high electron density, and very high saturation and peak drift velocities.[1,2] All these unique properties make InN a promising candidate to fabricate a wide range of devices such as tandem solar cells, IR emitters, and high-speed and high-frequency electronic devices. As a consequence of the great potential of InN for device applications, a great deal of effort has been devoted to improve the crystal quality of InN layers and numerous studies dealing with the optical and electrical properties of InN can be found in the literature.

High-pressure optical measurements are widely employed in semiconductor physics to obtain detailed information about the band structure and the lattice dynamics of semiconductors.[3] In particular, high-pressure techniques provide a highly useful benchmark to test existing models (for instance, density functional theory) for the calculation of the electronic and vibrational properties of semiconductors.

Several high-pressure Raman-scattering studies of wurtzite InN (w-InN) have been published so far.[4–7] Pinquier and coworkers[4,5] investigated the pressure dependence of the E_{2h}, A_1(TO), and LO phonons of w-InN. Pressure coefficients and mode Grüneisen parameters were obtained for these phonon modes, and the wurtzite-to-rocksalt transition was found to lie in the 12–14 GPa range, in agreement with

x-ray diffraction measurements[8] and with the predictions of *ab initio* calculations.[9] In Ref. 5 the pressure dependence of several broad features attributed to rocksalt InN (rs-InN) was investigated up to 50 GPa. However, it would be highly desirable to perform lattice-dynamical calculations as a function of pressure in order to support the assignment of the features that appear in the Raman spectra of rs-InN. In turn, Yao and coworkers[6] carried out high-pressure Raman-scattering measurements to study the structural stability of poorly crystalline w-InN nanowires. Recently the softening of the E_{2l} mode has been observed, and the pressure behavior of the E_1(TO) mode has been investigated on a-face layers,[7] with good agreement between the experimental data and *ab initio* calculations relying on density functional theory.

Despite these previous investigations, there are still open questions with regard to the high-pressure vibrational properties of InN. On the one hand, it has been shown that longitudinal optical (LO) modes with large wave vectors defined by the incoming photon energies are selectively excited in Raman-scattering experiments on w-InN.[10] The selective excitation of LO modes with large wave vectors, attributed to a double-resonance excitation process in which the phonon wave vector (q) depends on the electron-hole dispersion,[10] may strongly affect the pressure behavior of the LO modes in w-InN through pressure-induced changes of the electronic structure. On the other hand, a relatively large dispersion of pressure coefficients and mode Grüneisen parameters for both the polar and nonpolar modes of w-InN and w-GaN can be found in the literature. Given that the observed discrepancies could be in part related to residual strains in epilayer material, high-pressure Raman experiments on layers grown on different substrates and/or with different levels of residual strain could be highly informative.

In the case of heavily doped n-type samples, LO-plasmon coupling gives rise to long-wavelength ($q \simeq 0$) L^- modes.[11] While the number of studies dealing with the investigation of the pressure behavior of LO-plasmon coupled modes (LOPCMs) in III–V semiconductors is scarce,[12–14] the pressure dependence of the LOPCMs could be used to gain information about the electronic structure of these compounds.

Here we report Raman-scattering measurements under high hydrostatic pressure on five different w-InN epilayers grown on sapphire substrates. The experimental results are discussed in the light of *ab initio* lattice-dynamical calculations on both w-InN and rs-InN at different pressures. Good agreement is found between the experimental and calculated pressure coefficients of the zone center E_{2l}, E_{2h}, A_1(TO), and E_1(TO) phonons of w-InN. The role of residual strain on the measured pressure coefficients is shown to be negligible within the experimental error of these type of high-pressure measurements. The analysis of the pressure behavior of the LO band in w-InN, taking into account the double-resonance mechanism responsible for the selective excitation of LO phonons with large wave vectors in this material, indicates that the experimental pressure coefficients obtained under visible excitation are barely affected by pressure-induced changes of the electronic structure of w-InN. The pressure behavior of the L^- LOPCM that shows up in heavily doped n-type w-InN is investigated, and the frequency of the L^- band is used to evaluate the electron effective mass of w-InN as a function of hydrostatic pressure. The effective mass values thus obtained turn out to agree well with $\mathbf{k} \cdot \mathbf{p}$ theory. The wurtzite-to-rocksalt phase transition and the subsequent rocksalt-to-wurtzite backtransition are observed in the upstroke and downstroke cycles, respectively. The lattice-dynamical calculations are used to assign the different Raman features that appear in the spectra of both rs-InN and backtransited, poorly crystalline w-InN.

II. EXPERIMENT

For the present work, we used one a-face and four c-face InN epilayers grown by plasma-assisted MBE on sapphire substrates. The background electron density of the samples was obtained with Hall-effect measurements and ranges from $n_e \sim 1 \times 10^{18}$ to 1.6×10^{19} cm^{-3}. Table I shows the thickness and background electron concentration of the samples.

Flakes of w-InN containing residual sapphire were detached from the substrates by mechanical polishing and subsequent

TABLE I. List of samples studied in this work, including data about the residual electron concentration (n_e) and thickness of the w-InN epilayers. All samples are c-face material except sample D, which is a-face.

Sample	Structure	n_e ($\times 10^{18}$ cm^{-3})	Thickness (μm)
A	InN/GaN/sapphire	2	0.5
B1	InN/sapphire	6.5	0.4
B2	InN/sapphire	16	0.4
C	InN/sapphire	<2	5.7
D	InN/sapphire (a-face)	4	0.5

cutting. The flakes, together with a few ruby chips, were placed in a gasketed membrane-type diamond anvil cell (DAC) with 400 μm culet-size diamonds. Methanol-ethanol-water (16:3:1) was used as pressure transmitting medium, and the applied pressure was determined with the ruby fluorescence method.

Confocal micro-Raman measurements at room temperature were performed with a HORIBA Jobin-Yvon LabRam-HR spectrometer. The measurements were excited with the 632.8-nm line of a He-Ne laser, since this excitation wavelength allowed us to reduce the Rayleigh radiation and detect the low-frequency E_{2l} mode of w-InN. A 50$\times$ objective was employed to focus the laser beam and to collect the backscattered radiation.

III. *AB INITIO* CALCULATIONS

Ab initio lattice-dynamical calculations for w-InN and rs-InN were carried out at different hydrostatic pressures. The calculations were performed using a plane-wave pseudopotential approach to DFT as implemented in the ABINIT package.[15] The calculations were performed within the local density approximation (LDA) by using the Teter parametrization of the exchange-correlation functional[16] and Troullier-Martins pseudopotentials.[17] For the In pseudopotential, 4d electrons were included as valence states. An $8 \times 8 \times 4$ Monkhorst-Pack k-point sampling and a plane-wave basis set with energy cutoffs ranging from 65 to 100 Ha were considered.

A full structural relaxation of the w-InN crystal lattice at zero pressure yielded the following lattice parameters: $a = 3.520$ Å and $c = 5.691$ Å. These values are in very good agreement with those measured by high-resolution x-ray diffraction measurements.[18] Structural relaxation of the w-InN lattice as a function of pressure allowed us to determine the zero-pressure bulk modulus ($B_0 = 143$ GPa). This value is in good agreement with experimental measurements[19] and with previous first-principles calculations.[20] In the case of rs-InN, the full structural relaxation yielded a lattice parameter of $a = 4.523$ Å at ambient pressure and a zero-pressure bulk modulus of $B_0 = 186$ GPa, only slightly higher than the value measured by Uehara *et al.* (170 $\pm$ 16 GPa).[8] For hydrostatic pressures of $p = 15$ GPa, just above the transition pressure, we find a bulk-modulus value of $B_{15} = 255$ GPa. The resulting first pressure derivative of $B_0(p)$ is around 4.6, which is in good agreement with the value measured by Uehara *et al.* ($B'_0 = 5 \pm 0.9$).[8]

To obtain the phonon dispersion and phonon density of states over the whole Brillouin zone, the ABINIT code computes the dynamical matrix on a mesh of k points using the perturbation theory linear-response approach.[21,22] Interatomic force constants are generated at arbitrary wave vectors by a Fourier transformation, and the dynamical matrices and phonon frequencies are then interpolated for the whole Brillouin zone. Lattice-dynamical calculations were performed at different pressure values, and linear pressure coefficients (a_i) for the zone-center phonons of w-InN and rs-InN were thus obtained.

Figure 1 displays the calculated phonon dispersion along high-symmetry directions at pressure values $p = 0$ and 10 GPa for w-InN. Similarly, Fig. 2 shows the phonon dispersion at $p = 15$ and 25 GPa for rs-InN. The corresponding one-phonon
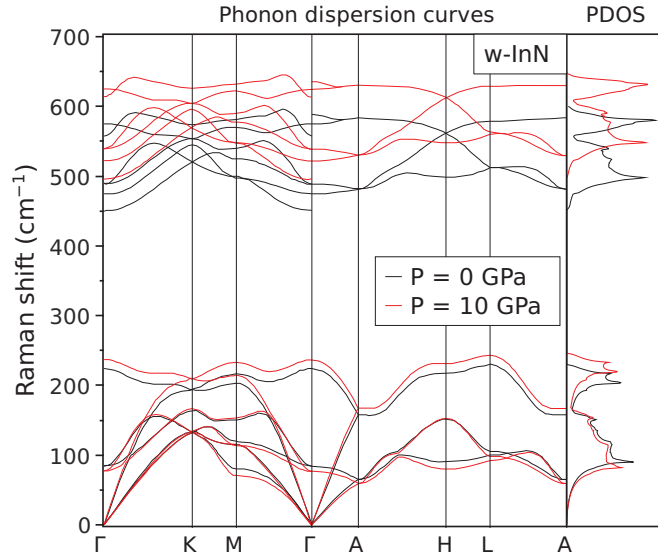
FIG. 1. (Color online) *Ab initio* calculation of the phonon band structure of wurtzite InN along the main lines of symmetry at 0 and 10 GPa. The right panel shows the corresponding phonon density of states (PDOS).
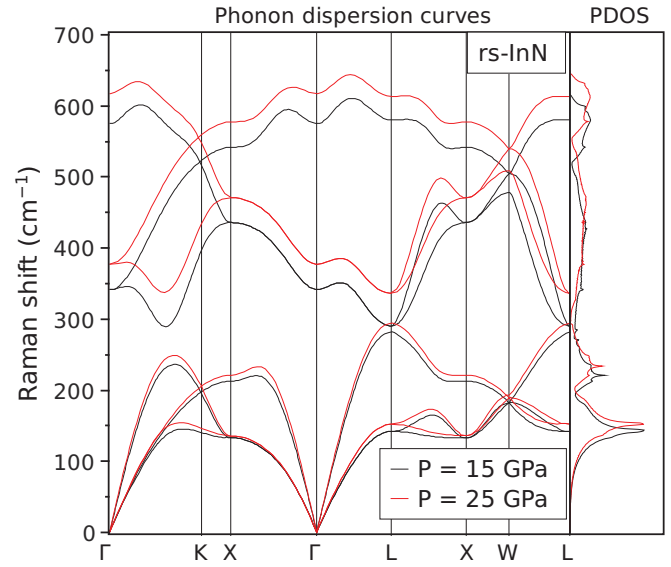

FIG. 2. (Color online) *Ab initio* calculation of the phonon band structure of rocksalt InN along the main lines of symmetry at 15 and 25 GPa. The right panel shows the corresponding phonon density of states (PDOS).

density-of-states (1-PDOS) curves are displayed in the right panel of both figures. As expected, the phonon branches and the calculated PDOS exhibit an overall upward frequency shift with increasing pressure, with the exception of the E_{2l} and transverse acoustic (TA) branches of w-InN, for which the DFT calculations predict a downward frequency shift with increasing pressure. The softening of these modes has been related to the stability of tetrahedral structures under pressure.[23,24] Conversely, the present DFT calculations do not predict any softening of the TA branches of rs-InN. The phonon frequencies at 0 GPa (ω_{i0}), linear pressure coefficients (a_i), and mode Grüneisen parameters ($\gamma_i = B_0 a_i/\omega_{i0}$) for the zone-center optical modes of w-InN and rs-InN as obtained from the present DFT calculations are displayed in Tables II and III, respectively. In the case of rs-InN, the calculations were also performed around $p = 15$ GPa to obtain the corresponding

pressure coefficients and Grüneisen parameters around the phase transition pressure (Table III). Note that, although structural techniques show that the phase transition in InN starts around 12 GPa, optical experiments show that the transition is complete only above 15 GPa.[25] The Grüneisen parameters at 15 GPa were computed by using the bulk modulus at this pressure value ($B_{15} = 255$ GPa). As can be seen in Table III, the calculated a_i values around 15 GPa for rs-InN are sizably lower than those obtained at 0 GPa, reflecting the decreasing compressibility of the material with increasing p.

As discussed elsewhere,[26] the ABINIT code provides a good convergence of the phonon frequencies except for the LO modes. This limitation, which may be related to uncertainties in the values of the dielectric constant arising from the LDA band-gap problem, yields an incorrect ordering of the $A_1(LO)$ and $E_1(LO)$ phonon frequencies in w-InN and also a spurious

TABLE II. Best values for the zero-pressure frequency (ω_{i0}), linear pressure coefficient ($a_i = d\omega_i/dp$), relative pressure coefficient ($d \ln \omega_i/dp = a_i/\omega_{i0}$), and mode Grüneisen parameters ($\gamma_i = a_i B_0/\omega_{i0}$) for the zone center TO and E_2 optical phonons and the LO band of w-InN as obtained from high-pressure Raman scattering measurements on different w-InN samples. For comparison, values obtained with *ab initio* lattice-dynamical calculations are also given. Theoretical data for the LO band correspond to the zone-center $A_1(LO)$ mode. A zero-pressure bulk modulus of 143 GPa was used to obtain the γ_i values.

Phonon mode (i)	$\omega_{i0}(\text{cm}^{-1})$	$a_i(\text{cm}^{-1}\text{GPa}^{-1})$	$d \ln \omega_i/dp(\text{GPa}^{-1})$	γ_i
E_{2l} (theor.)	83.9	-0.63	-0.0075	-1.07
E_{2l} (expt.)	88	-0.35 ± 0.05	-0.004 ± 0.0006	-0.6 ± 0.09
$A_1(TO)$ (theor.)	450.4	4.69	0.0104	1.49
$A_1(TO)$ (expt.)	449	5.3 ± 0.5	0.012 ± 0.001	1.69 ± 0.16
$E_1(TO)$ (theor.)	474.5	4.88	0.0103	1.47
$E_1(TO)$ (expt.)	476	5.3 ± 0.5	0.011 ± 0.001	1.59 ± 0.16
E_{2h} (theor.)	488.4	5.18	0.0106	1.52
E_{2h} (expt.)	489	5.1 ± 0.3	0.0104 ± 0.0006	1.49 ± 0.09
$A_1(LO)$ (theor.)	591.8	4.87	0.0082	1.18
LO (expt.)	595	4.8 ± 0.4	0.0081 ± 0.0007	1.15 ± 0.1

TABLE III. Theoretical values for the zero-pressure frequency (ω_{i0}), linear pressure coefficient (a_i) at 0 GPa and the corresponding mode Grüneisen parameters (γ_i) for the zone-center optical phonons of rs-InN as obtained with *ab initio* lattice-dynamical calculations. Values around 15 GPa, corresponding to hydrostatic pressures just above the transition pressure, are also given. Bulk modulus values of 186 and 255 GPa at 0 and 15 GPa obtained from the present DFT calculations were used to calculate the γ_i values.

Phonon mode (i)	ω_{i0}	$a_i(\text{cm}^{-1})$	$\gamma_i(\text{cm}^{-1}\text{GPa}^{-1})$
TO (0 GPa)	268.7	5.78	4.00
TO (15 GPa)	340.0	3.99	3.00
LO (0 GPa)	530.4	5.35	1.88
LO (15 GPa)	597.5	3.80	1.62

dispersion of the $E_1(\text{LO})$ branch along the Γ-M and Γ-K high-symmetry lines. Similarly, as also reported in the case of other rocksalt compounds like CdO,[27] large errors for the frequency and dispersion of the LO mode of rs-InN may be expected. These errors pose some limits to the accuracy of the calculated 1-PDOS and will have to be borne in mind for the discussion of the high-pressure Raman data presented later.

IV. RESULTS AND DISCUSSION

In Raman-scattering experiments on w-InN material, three types of excitations may be expected to appear in the first-order spectra: (1) zone-center ($q \simeq 0$) nonpolar (E_{2l} and E_{2h}) modes and polar (A_1 and E_1) TO modes, excited through the deformation potential mechanism; (2) polar (A_1 and E_1) LO modes with large wave vectors ($q \neq 0$) defined by the exciting photon energies through a double-resonance excitation process;[10] (3) the long-wavelength ($q \sim 0$) L^- branch of the LOPCMs.[11,28,29]

The pressure behavior of all these modes might be affected by residual strains in the epilayers. In addition, the pressure dependence of non-Γ LO modes may be modified by pressure-

FIG. 4. (Color online) Raman spectra acquired at different hydrostatic pressure values from a heavily doped *n*-type w-InN epilayer grown on sapphire (sample B2).

induced changes of the electronic structure of w-InN. In the case of the L^- modes, the pressure dependence is expected to reflect pressure-induced changes of both the bare phonon frequencies and of the electron effective mass.

Figures 3–5 show selected high-pressure Raman spectra of InN. The spectra of Fig. 3 correspond to a high-quality InN epilayer grown on a GaN template (sample A). The Raman spectra of Fig. 4 were obtained from a heavily doped *n*-type epilayer directly grown on sapphire (sample B2), while those of Fig. 5, measured up to 19.6 GPa (i.e., beyond the wurtzite-to-rocksalt transition), correspond to a 5.7-μm-thick (relaxed) InN epilayer (sample C). In Ref. 7 Raman spectra below 10 GPa were reported for this sample and also for the a-face InN epilayer (sample D).

As expected from the Raman selection rules for c-face wurtzite crystals, below the wurtzite-to-rocksalt phase transition all the spectra of w-InN are dominated by the nonpolar E_{2l}
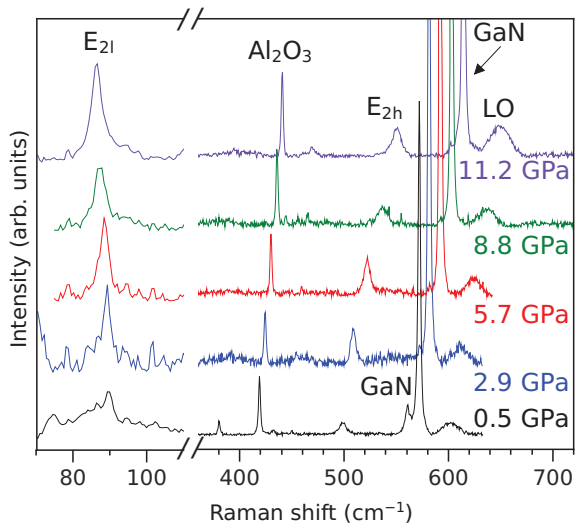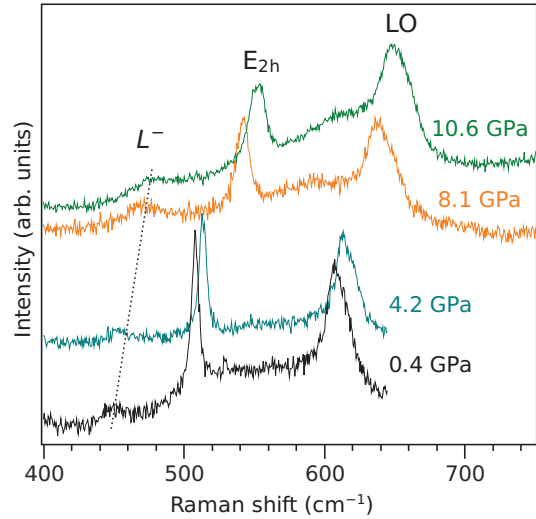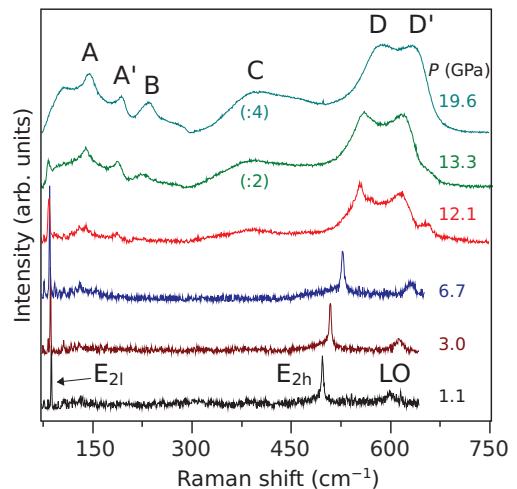

FIG. 3. (Color online) Raman spectra acquired at different hydrostatic pressure values from a high-quality w-InN epilayer grown on a GaN template (sample A).

FIG. 5. (Color online) Raman spectra acquired at different hydrostatic pressure values, up to 20 GPa, from a 5.7-μm-thick epilayer grown on sapphire (sample C).
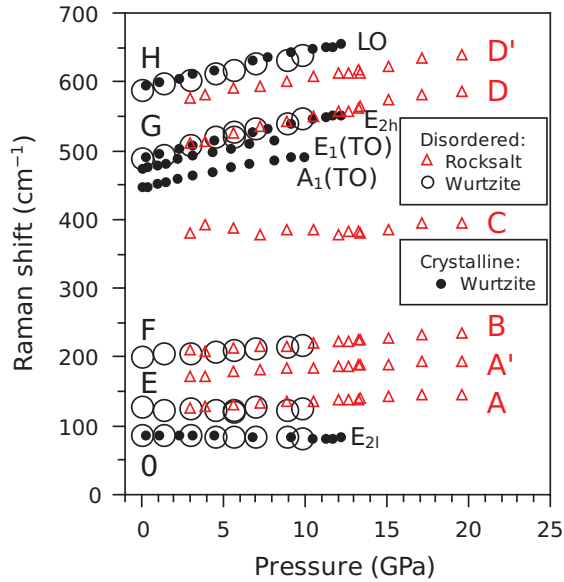
FIG. 6. (Color online) Pressure dependence of the optical phonon frequencies of crystalline wurtzite InN measured in the up-stroke cycle in c-face InN and a-face InN (solid dots). The triangles show the pressure dependence of the disorder-activated first-order bands that appear in the Raman spectrum of rocksalt InN in the up-stroke and in the down-stroke cycles (bands A to D′). The open circles show the corresponding data points for the disorder-activated first-order bands that show up in the Raman spectra after the rocksalt-to-wurtzite backtransition (bands O and E to H).

and E_{2h} phonons (Figs. 3–5). In the case of sample A, grown on GaN/sapphire, strong peaks from GaN are also observed (Fig. 3). In the high-frequency region, a weak band arising from the $q \neq 0$ A_1-E_1 LO phonons of w-InN is also observed in all samples. As discussed in Ref. 7, the Raman spectra of the InN flakes loaded into the DAC contain contributions of both A_1 and E_1 symmetries, which is attributed to symmetry-forbidden enhancement of the E_1(LO) signal due to the impurity-induced Fröhlich interaction mechanism.[11] In the case of a-face material (sample D), the Raman spectra also exhibit weak features corresponding to the zone-center A_1(TO) and E_1(TO) modes (not shown here; see Ref. 7).

The pressure dependence of the phonon modes that is typically obtained in w-InN is illustrated in Fig. 6 (plotted with solid dots). The figure shows the pressure dependence of the E_{2l}, E_{2h}, and LO frequencies as obtained during the upstroke cycle for the thick (relaxed) InN epilayer (sample C). As will be discussed below, a virtually equivalent pressure behavior was observed for the rest of samples. For completeness, the figure also shows the pressure dependence of the TO modes measured on the a-face epilayer (sample D). From a linear fit to the data, zero-pressure frequencies, ω_{i0}, and hydrostatic linear pressure coefficients, $a_i = (d\omega_i/dp)_{p=0}$, can be extracted for the ith phonon mode. The values obtained throughout this work (see below) are summarized in Table II.

A. Zone-center phonons: E_{2l}, E_{2h}, and TO modes

The pressure behavior of the zone-center E_{2l}, E_{2h}, and TO modes was previously investigated in Ref. 7, where the
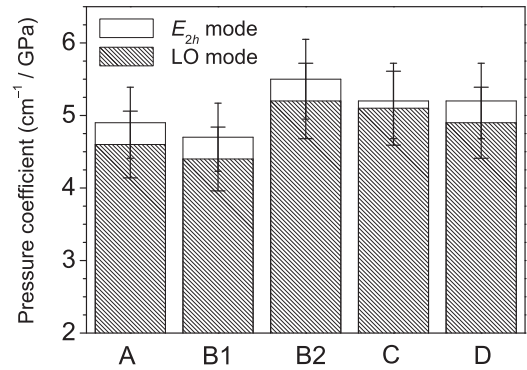

FIG. 7. Pressure coefficients for the E_{2h} and LO bands as obtained with high-pressure Raman measurements on all the samples investigated in this work. Error bars have been added to both plots.

softening of the E_{2l} was observed and the pressure coefficients of the TO modes were measured. However, the experimental pressure coefficients of the zone-center phonon modes of w-InN could be strongly affected by strain-related phenomena. Indeed, InN epilayers grown on sapphire or GaN/sapphire substrates usually display different degrees of compressive strain.[28,30] Also, the compressibility of the sapphire substrate is markedly lower than that of InN or GaN. As a consequence, the application of pressure on the InN epilayers could partly compensate the built-in compressive strains and give rise to reduced phonon pressure coefficients in comparison to relaxed material. In order to investigate the effect of built-in strains on the high-pressure Raman spectra of w-InN epilayers, we have investigated five different InN samples (see Table I). These measurements were partly motivated by the fact that, in spite of the small number of works dealing with the high-pressure vibrational properties of w-InN[4–7] and of w-GaN,[31–34] the dispersion of reported pressure-coefficient values in these two compounds is relatively high. For instance, in the case of the E_{2h} mode of w-InN, pressure coefficients ranging from 4.74 cm^{-1} GPa^{-1} (Ref. 6) up to 5.56 cm^{-1} GPa^{-1} (Ref. 4) have been reported.

Figure 7 shows the linear pressure coefficients measured for the zone-center E_{2h} modes in all the samples investigated in this work. Data for the LO modes (see discussion below) are also given. As can be seen in the figure, slightly different values are obtained in these epilayers. The observed variations, however, do not seem to display any clear trend with regard to the sample thickness and/or the residual strain of the epilayers (the latter can be readily evaluated from the zero-pressure E_{2h} frequency).[28,30] This can be seen by comparing the pressure coefficient of sample A, which exhibits the highest degree of compressive strain among all the samples investigated, with that of samples B1 and B2, with similar degrees of strain relaxation. Similarly, in spite of their sizably different degrees of strain, the pressure coefficients of the 5.7-μm-thick (relaxed) epilayer (sample C) and that of the a-face epilayer (sample D) are very similar. The observed variations are in all cases lower than the expected error of this type of measurements, which may be taken around $\sim 10\%$. Typical sources of error in these experiments may arise from pressure gradients within the gasket, which may be particularly important when the sample is located at a relatively large

distance from the ruby chips. Thus, we conclude that within the experimental error of the technique, the measured pressure coefficients are not affected by built-in compressive strains in the epilayers.

In the case of the w-InN epilayer grown on GaN/sapphire (sample A), strong peaks corresponding to the A_{1g} mode of sapphire and the E_{2h} and E_1(TO) modes of GaN also show up in the Raman spectra (see Fig. 3). We obtain a pressure coefficient of 2.0 ± 0.2 cm^{-1} GPa^{-1} for the A_{1g} mode of sapphire, in good agreement with previous results (2.1 cm^{-1} GPa^{-1} in Ref. 35). In the case of GaN, we measure a linear pressure coefficient of 3.7 and 3.9 cm^{-1} GPa^{-1} for the E_1(TO) and E_{2h} modes of GaN, respectively. These values agree well with the data published in the literature: for the E_1(TO) mode, values of 3.68 cm^{-1} GPa^{-1} (Ref. 31) and 3.94 cm^{-1} GPa^{-1} (Ref. 34) were measured on GaN single crystals and on 50-μm-thick GaN crystals grown on SiC, respectively. In the latter reference, a value of 3.3 cm^{-1} GPa^{-1} obtained with DFT calculations was also given. In the case of the E_{2h} mode of w-GaN, somewhat larger experimental pressure coefficients have been reported (4.17 cm^{-1} GPa^{-1} in Ref. 31 and 4.24 cm^{-1} GPa^{-1} in Ref. 34). In this case, the *ab initio* lattice-dynamical calculations predict a value of 3.6 cm^{-1} GPa^{-1},[34] only slightly lower than our experimental value. As in the case of the E_{2h} mode of w-InN discussed above, the present results seem to confirm that the dispersion of the pressure coefficients that can be found in the literature for w-GaN is not a consequence of strain but of the intrinsic experimental error of this type of measurements.

From the set of data obtained from all our measurements for the E_{2h} of w-InN, collected in the histogram of Fig. 7, and also from the measurements for the E_{2l} mode, we obtain best values for the linear pressure coefficients (a_i) and the corresponding mode Grüneisen parameters, $\gamma_i = B_0 a_i / \omega_{i0}$, of these two modes. Table II summarizes the values thus obtained. A value of $B_0 = 143$ GPa as obtained from the DFT calculations has been used to calculate γ_i. The table also shows data for the TO phonons as measured on the a-face epilayer (sample D). In addition, Table II displays ω_{i0} values for the different zone-center modes of w-InN. For the E_{2l} and E_{2h}, the data correspond to strain-free w-InN material (sample C). In the case of the TO phonons, the ω_{i0} values displayed in the table were obtained from a compressively strained epilayer (sample D). Thus, these values are somewhat larger than the experimental values expected in strain-free w-InN.

For comparison, Table II also shows the corresponding results of the DFT-LDA lattice-dynamical calculations described in Sec. III. As can be seen in the table, overall good agreement is found between the experimental and calculated a_i values for the E_2-symmetry modes. In particular, as discussed in Ref. 7, the DFT calculations predict the softening of the E_{2l} mode in w-InN. On the other hand, the calculated a_i values for the TO modes are only slightly lower than those obtained experimentally.

The relative pressure coefficients of the zone-center phonons, $d \ln \omega_i(p)/dp$, can be linked to those of the nearest-neighbor bond lengths involved in the different vibrations.[36] For instance, the relative pressure coefficients of E_1(TO) and E_{2h} phonons in w-InN are very similar (see Table II) because both modes involve vibrations in the hexagonal plane.

A direct comparison of the $d \ln \omega_i(p)/dp$ values obtained from the present measurements with those of w-GaN and w-AlN (see data in Ref. 36) confirms that, owing to the higher compressibility of w-InN, $d \ln \omega_i(p)/dp$ is sizable larger in this compound. In the particular case of the A_1(TO) mode, the higher $d \ln \omega_i(p)/dp$ value in w-InN in relation to w-GaN and w-AlN arises from the higher relative pressure coefficient of the bonds along the c axis.[36] In the case of the E_1(TO) and E_{2h} modes, the higher relative pressure coefficient of the bond lengths of w-InN within the hexagonal plane also gives rise to higher $d \ln \omega_i(p)/dp$ values in comparison to w-GaN and w-AlN.

Both the measured and calculated pressure coefficients for the A_1(TO) and the E_1(TO) modes, with ionic vibrations in nonequivalent directions, turn out to be very similar (see Table II). This result can be interpreted in terms of a small structural anisotropy in w-InN, i.e., a small deviation of the axial ratio c/a of the hexagonal cell in relation to its ideal value (1.633). This is in contrast to the case of w-AlN, which displays sizable degrees of structural anisotropy, as shown by DFT calculations and confirmed by the relatively large pressure dependence of the A_1-E_1 TO splitting.[36] In the case of w-InN, the fact that the A_1-E_1(TO) splitting barely depends on p points to a small pressure dependence of the structural anisotropy in this compound. This is in agreement with the structural data of Ueno *et al.*, who found a very small decrease of the c/a ratio in w-InN below 10 GPa.[19]

B. LO phonons with large wave vectors

Davydov *et al.*[10] showed that in Raman-scattering experiments on w-InN, A_1(LO) and E_1(LO) modes with large wave vectors are selectively excited. This observation, also reported in w-InN nanowires,[37] was attributed to a double-resonance excitation process that occurs due to the unusual conduction band of w-InN. Within this interpretation, the wave vector conservation law is broken due to scattering of electrons and holes from charged impurity centers. The wave vectors of the phonons are defined by the exciting photon energies, E_{exc}, so that the magnitude of the phonon wave vector (q) is given by twice the wave vector in the electron-hole dispersion corresponding to an energy equal to E_{exc}, i.e., $q = 2k$, with

$$E_{exc} = E_g(p) + E_e(k) - E_h(k), \qquad (1)$$

where $E_g(p)$ is the pressure-dependent band-gap energy of w-InN, and $E_e(k)$ [$E_h(k)$] is the conduction (light-hole or heavy-hole) band dispersion. According to the results of Ref. 10, the q values for A_1(LO) modes are determined by the electron-light hole dispersion, while those of E_1(LO) phonons are given by electron-heavy hole transitions.

One important implication of this model is that the LO phonon wave vector should be modified by pressure-induced changes of the electronic structure, which should have a bearing on the experimental pressure coefficients of the LO modes of w-InN. With regard to this, it can be realized that the pressure coefficient of the LO modes with large q values can be separated into two different contributions,
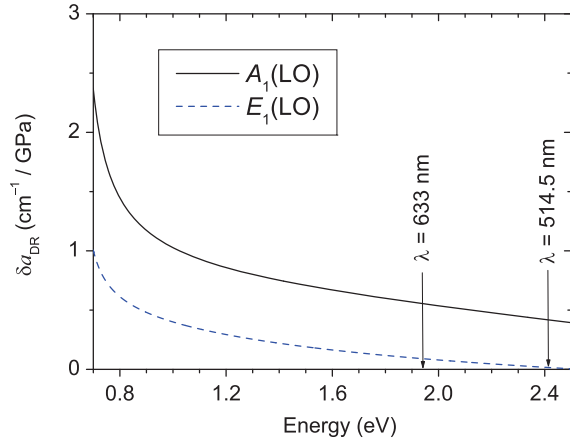
$$a_{LO} = \frac{d\omega_{LO}}{dp} + \delta a_{DR}, \qquad (2)$$

FIG. 8. (Color online) Change of the LO-phonon pressure coefficient, δa_{DR}, as a function of the excitation energy for A_1(LO) and E_1(LO) phonons. δa_{DR} takes into account pressure-induced variations of the frequency of LO modes with large wave vectors as a consequence of the double-resonance excitation of these modes.

where $d\omega_{LO}/dp$ refers to the conventional pressure dependence expected for optical phonons as a consequence of the compression of the lattice, while δa_{DR} takes into account pressure-induced variations of the LO frequency as a consequence of the wave-vector change induced by the double-resonance excitation.

Figure 8 illustrates the excitation energy dependence of δa_{DR} that predicts the model of Ref. 10 for the A_1(LO) and E_1(LO) phonons. Note that these curves have been obtained within a simplified framework, and, as a consequence, they should be taken only as a qualitative guide to illustrate the pressure behavior of the LO phonons of w-InN that might be expected from the selective excitation mechanism proposed in that work. To calculate the curves of Fig. 8 we first obtained the pressure-induced phonon wave-vector variation for a given E_{exc} value by taking pressure derivatives of the resonance condition Eq. (1). The pressure-induced wave-vector variation, dk/dp, was numerically evaluated, and the corresponding pressure derivatives for the A_1(LO) and E_1(LO) modes were subsequently calculated by using the numerical phonon dispersions obtained in Ref. 10. Note that pressure yields an overall uniform frequency increase of the optical phonon frequencies along the whole Brillouin zone, equivalent to that of zone-center phonons [i.e., $d\omega_{LO}(\Gamma)/dp$], with no important wave-vector dispersion variations. This can be seen in Fig. 1 by comparing the dispersion of optical phonons at 0 and 10 GPa. Note that, in contrast, the acoustic modes display sizable changes in the phonon dispersion as expected due to the stiffening of the elastic constants with increasing pressure.

Following Ref. 10, the electron and the light-hole band dispersions were calculated within a **k · p** approach that includes nonparabolicity effects, i.e., $E_e(k) = E_e\{\sqrt{\hbar^2 k^2 / 2m_e^*(p)E_e + 1/4} - 1/2\}$ and $E_{lh}(k) = -E_{lh}\{\sqrt{\hbar^2 k^2 / 2m_{lh}^*(p)E_{lh} + 1/4} - 1/2\}$, where E_e and E_{lh} are nonparabolicity coefficients and $m_e^*(p)$ and $m_{lh}^*(p)$ are pressure-dependent electron and light-hole effective masses at the Γ point. As in Ref. 10, a parabolic heavy-hole

dispersion was assumed. For these calculations, pressure-induced changes of the light-hole and heavy-hole effective masses were neglected for simplicity. The pressure dependence of m_e^* can be modeled within a **k · p** formalism as

$$\frac{m_e^*(p)}{m_e^*(0)} = \frac{E_g(p)}{E_g(0)}, \quad (3)$$

where $m_e^*(0) = 0.07m_e$ is the ambient-pressure effective electron mass at Γ (Ref. 2), $E_g(p) = E_g(0) + a_g p$ is the pressure-dependent fundamental band-gap energy of w-InN, $E_g(0)$ is the ambient-pressure band-gap energy, and a_g is the pressure coefficient of the fundamental band-gap. In the case of undoped w-InN, $E_g(0) = 0.65$ eV and $a_g = 32$ meV/GPa,[25] which yields a relative pressure coefficient for the electron effective mass, $\gamma_m = (d\ln m_e^*(p)/dp)_{p=0}$, equal to 0.0492 GPa^{-1}. According to Eq. (3) and using the band-gap pressure coefficients obtained in Ref. 25 as a function of n_e, γ_m decreases to 0.0312 GPa^{-1} for $n_e = 1.6 \times 10^{19}$ cm^{-3} as in our most heavily doped sample. These values are similar to those determined with pressure-dependent mobility measurements on w-InN.[38]

According to the above considerations, the dk/dp changes arise from the pressure-induced increase of both the band-gap energy and the effective masses. The opening of the band-gap with hydrostatic pressure implies a reduction of the corresponding phonon-wave vector for a fixed photon energy, and, as a consequence, it yields positive δa_{DR} values. The increase in the electron effective mass yields the opposite effect. This is reflected in Fig. 8 for the case of undoped material, which shows that δa_{DR} is clearly larger around the fundamental band gap of w-InN, i.e., where nonparabolicity effects are less important. With increasing excitation energy, the reduction of δa_{DR} induced by the increase of effective mass counteracts the effect arising from the pressure-induced band-gap opening.

As can be seen in Fig. 8, the predicted variation of the linear pressure coefficients of the A_1(LO) and E_1(LO) phonons of w-InN induced by the doubly resonant selective excitation of both modes, $d\omega_{DR}/dp$, is larger for the A_1(LO) phonon. This occurs as a consequence of the lower magnitude of the wave vectors involved in the selective excitation of this mode.[10] As can be seen in the figure, this model predicts δa_{DR} values of around 1 and 2.5 cm^{-1} GPa^{-1} for the E_1(LO) and A_1(LO) modes, respectively, for excitation energies around the fundamental band gap of InN. With increasing excitation energy, the effect on the phonon pressure coefficients is rapidly reduced. For the photon energies corresponding to the wavelength employed in the present work (632.8 nm), the model predicts that $\delta a_{DR} \sim 0.5$ cm^{-1} GPa^{-1} for the A_1(LO) mode and a value close to zero for the E_1(LO) phonon.

Bearing in mind the A_1-E_1 character of the LO bands, it can be concluded that the experimental pressure coefficients of the large wave-vector LO modes measured in this work are barely affected by the double-resonance mechanism, i.e., $a_{LO} \approx d\omega_{LO}/dp$. However, the present calculations do suggest that high-pressure Raman measurements on w-InN samples excited with markedly different wavelengths (for instance, longer wavelengths vs UV excitations) could give rise to sizable changes in the measured LO-phonon pressure

coefficients. Thus, this type of experiments could be highly informative with regard to the selective excitation of LO modes with large wave vectors in w-InN.

As in the case of the E_{2h} phonons, from the set of data obtained from all our measurements for the LO band (see Fig. 7) we obtain the average value for the linear pressure coefficient (a_i) and the corresponding mode Grüneisen parameter, $\gamma_i = B_0 a_i / \omega_{i0}$, of this mode. The value thus obtained is shown in Table II. Following the previous considerations, we conclude that the effect of the double-resonance mechanism on this value, measured with 632.8 nm radiation, is within the experimental error of this type of high-pressure experiments.

C. Long-wavelength L^- coupled modes

In polar semiconductors, free carriers couple with LO phonons and give rise to the L^+ and L^- LO-plasmon coupled modes (LOPCMs). Numerous studies have been reported on inelastic light scattering by LOPCMs in III–V semiconductors, and different models have been developed to analyze the LOPCM behavior.[39–41] The analysis of the LOPCM peaks is widely employed to evaluate in a contactless and nondestructive manner the free-carrier density of the samples. However, only a few reports have been devoted to investigate the pressure dependence of the LOPCMs.[12,13]

In the case of the heavily doped, n-type w-InN sample studied in this work (sample B2), in addition to the E_2 and LO modes, a peak corresponding to the L^- LOPCM also shows up in the Raman spectra (see Fig. 4). It has been shown that wave vector is conserved in Raman scattering by the L^- coupled-modes in high-quality w-InN. These modes exhibit the usual behavior of the low-energy branch of the long-wavelength ($q \sim 0$) LOPCMs, i.e., they increase in frequency and phononlike character with increasing electron density.[11,29] The dependence of the L^- mode on carrier concentration can be satisfactorily described with the standard dielectric model,[39,40] and line-shape fits to the L^- peak allow one to extract free-electron density values in good agreement with Hall-effect measurements.[11,28] In contrast, L^+ bands do not show up in the Raman spectra, which may be attributed to the low Raman-scattering efficiencies of this mode in the III-nitrides as well as to electron density inhomogeneities.[11] It should be noted that in the last decade there was some controversy with regard to the simultaneous observation of LO phonons and L^- coupled modes in w-InN. In fact, some authors tentatively explained the appearance of the LO peaks in doped samples through $q \neq 0$ LOPCMs excited by breakdown of the Raman selection rules[42–44] or by a Fano-type interference between the LO mode and the continuum electronic states.[45] According to the results of Refs. 10 and 11, the simultaneous observation of LO and L^- modes in doped material is a consequence of the different wave vectors involved: large wave vectors in the case of the A_1-E_1 LO modes due to the double-resonance excitation, and $q \sim 0$ wave vectors for the L^- coupled modes.

The aim of this section is to study the pressure dependence of the long-wavelength L^- mode in sample B2 ($n_e = 1.6 \times 10^{19}$ cm^{-3}) in order to evaluate the electron effective mass of w-InN as a function of pressure. Figure 9 shows the frequency
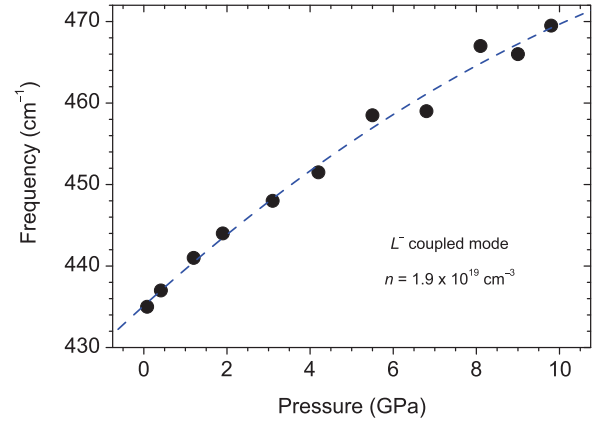

FIG. 9. (Color online) Frequency of the L^- coupled mode (solid dots) as obtained with high-pressure Raman measurements on a heavily doped n-type w-InN epilayer (sample B2). The dashed line serves as a guide to the eye.

of the L^- peak as a function of applied hydrostatic pressure (solid dots) as obtained from the high-pressure measurements on sample B2. As can be seen in the figure, the L^- mode exhibits the expected blueshift with increasing hydrostatic pressure. In the low-pressure regime, below 4 GPa, the linear pressure coefficient of the L^- is ~4.3 cm^{-1}/GPa, which is markedly lower than that of the TO and LO phonons (see Table II). Thus, it is seen that in spite of its strong phononlike character, the L^- frequency reflects the expected increase of the electron effective mass with increasing pressure. At higher pressures, the figure shows a slight saturation of the linear dependence that we tentatively attribute to a reduction of the free-electron density by compensating defects generated during the pressurization of the sample.

To evaluate the electron effective mass, $m_e^*(p)$, from the Raman spectra we first note that the frequency of the long-wavelength L^- mode at a given pressure depends on the electron density, on the frequency of the zone-center TO and LO phonons and on $m_e^*(p)$. Thus, given that the pressure behavior of the TO and LO modes is already known, $m_e^*(p)$ at a given p value can be obtained from the frequency of the $q \sim 0$ L^- mode by using the expression[39]

$$\omega_-^2 = \tfrac{1}{2}\big\{(\omega_p^2 + \omega_{\rm LO}^2) - \big[(\omega_p^2 - \omega_{\rm LO}^2)^2 - 4\omega_p^2(\omega_{\rm TO}^2 - \omega_{\rm LO}^2)\big]^{(1/2)}\big\},$$

(4)

where $\omega_p^2(p) = 4\pi e^2 n_e / \epsilon_\infty m_e^*(p)$ is the pressure-dependent plasma frequency of the free carriers, and $\epsilon_\infty = 6.7$ is the high-frequency dielectric constant of w-InN.[46] For simplicity, we neglect the pressure dependence of ϵ_∞. In Eq. (4) $\omega_{\rm TO}$ and $\omega_{\rm LO}$ correspond to the zone-center TO and LO frequencies, respectively. The pressure dependence of both modes has been studied in the previous sections.

Then $m_e^*(p)$ values are estimated from the experimental L^- frequencies and Eq. (4) by assuming that n_e does not depend on p. Figure 10 (solid dots) shows the m_e^* values thus obtained. Around ambient pressure, the $m_e^*(p)$ values obtained from the L^- frequency are around $0.1m_e$, only slightly lower than the value extracted from a two-band $\mathbf{k} \cdot \mathbf{p}$ Kane model for w-InN
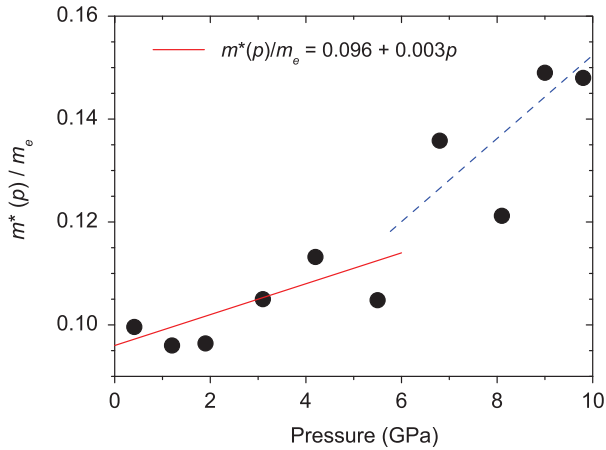
FIG. 10. (Color online) Electron effective mass values obtained from the frequency of the L^- mode as a function of pressure (solid dots). The solid line shows the result of a linear fit to the experimental data below 6 GPa, while the dashed line serves as a guide to the eye to the experimental points obtained at higher hydrostatic pressures.
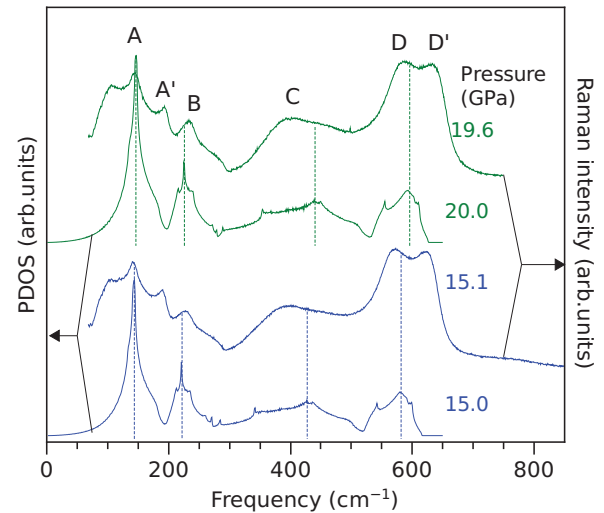

FIG. 11. (Color online) Raman spectra of rocksalt InN at 15.1 and 19.6 GPa. For comparison, calculated one-phonon density of states (PDOS) curves at 15 and 20 GPa for rs-InN are also shown.

with $n_e = 1.6 \times 10^{19}$ cm^{-3} ($m_e^* = 0.12m_e$).[28,47] In Ref. [48], line-shape fits to the L^- coupled mode of w-InN were carried out to estimate the ambient-pressure effective mass in samples with n_e just below 10^{19} cm^{-3}. Whereas the value obtained in that work ($m_e^* = 0.05m_e$) is clearly lower than that expected in heavily doped material, our result seems to better reflect the strong nonparabolicity of w-InN.[47]

As can be seen in Fig. [10], in the low-pressure regime ($p < 6$ GPa) the values of m_e^* obtained from Eq. [(4)] tend to increase linearly, in agreement with that expected from a $\mathbf{k} \cdot \mathbf{p}$ approach as discussed above [see Eq. [(3)]]. In contrast, at larger pressure values the figure shows a superlinear increase that most probably reflects a reduction of n_e in the pressurized sample due to the generation of compensating defects. A linear fit to the m_e^* values obtained below 6 GPa yields $m_e^*(p) = (0.096 + 0.003p)m_e$, which implies a relative pressure coefficient $\gamma_m = 0.031 \pm 0.01$ GPa^{-1}. This value is in excellent agreement with that obtained with Eq. [(3)] together with the data of Ref. [25] ($\gamma_m = 0.0312$ GPa^{-1} at $n_e = 1.6 \times 10^{19}$ cm^{-3}) and with that expected from the experimental results of Ref. [38], where a slightly larger value of $\gamma_m = 0.034$ GPa^{-1} was measured in samples with lower electron densities ($n_e = 2.4 \times 10^{18}$ cm^{-3}). Note, however, the large error associated to the determination of γ_m from the analysis of the L^- frequencies, suggesting that the nearly perfect match between the derived γ_m value and $\mathbf{k} \cdot \mathbf{p}$ theory may be fortuitous. In addition, it should be borne in mind that the pressure dependence of ϵ_∞ has been neglected for the present analysis. According to DFT-LDA calculations of the refractive index of w-InN as a function of pressure,[49] ϵ_∞ might display a sizable large (negative) pressure coefficient, much larger than that of w-GaN or w-AlN. Such pressure dependence would imply that the m_e^* values obtained from the frequency of the L^- modes have been underestimated. An experimental measurement of the pressure behavior of ϵ_∞ would be necessary in order to obtain a more reliable γ_m value extracted from the analysis of the L^- mode.

D. Raman scattering in rs-InN

Previous high-pressure Raman-scattering investigations have shown that, above ∼13 GPa, new bands that can be attributed to the rocksalt phase emerge in the Raman spectra of InN.[5,6] This can be observed in Fig. [5] for the case of sample C. In the spectrum obtained at 12.1 GPa, it can be seen that the phonons of w-InN coexist with new bands that are assigned to rs-InN. Note, however, that, as already mentioned, the phase transition is only complete around 17 GPa as observed by absorption spectroscopy.[25] The new Raman bands, which are labeled A, A′, B, C, D, and D′ in Fig. [5], totally dominate the Raman spectra well above the phase transition pressure. The Raman spectra plotted in the figure are very similar to those of previous works.[5,6] In Ref. [5], were Raman measurements of rs-InN were performed up to 50 GPa, it was found that features D and D′ merge above 30 GPa. It must be noted that similar Raman spectra were also measured in GaN[33] and AlN[36] above 30 and 20 GPa, respectively.

In crystalline materials with rocksalt structure one expects that first-order Raman modes are forbidden due to Raman selection rules. Thus, one would expect relatively weak bands arising from second-order modes. In the case of rs-InN, the frequency position of the observed features suggests that the spectra are dominated by first-order scattering, activated by the relaxation of the selection rules. We plot in Fig. [11] Raman spectra of rs-InN (sample C) at two different pressure values (15.1 and 19.6 GPa), together with calculated one-phonon DOS curves at similar pressure conditions (15 and 20 GPa). As can be seen in the figure, a remarkable qualitative agreement is found between the experimental data and the calculated curves, thus confirming that disorder-activated first-order modes dominate the Raman spectra of rs-InN after the wurtzite-to-rocksalt transformation. It is concluded that poorly crystalline (amorphized) rs-InN is formed after the phase transition.

Following the results of Fig. [11] and the corresponding phonon dispersion curves for rs-InN (see also Fig. [2]), features A and A′ can be attributed to disorder-activated transverse

TABLE IV. Zero-pressure frequency (ω_{i0}, linear pressure coefficient ($a_i = d\omega_i/dp$) and mode Grüneisen parameters ($\gamma_i = a_i B_0/\omega_{i0}$) for the different features that show up in the Raman spectra of rs-InN. A bulk modulus of 186 GPa was used to compute γ_i.

Feature (i)	Assignment	ω_{i0} (cm^{-1})	a_i (cm^{-1}GPa^{-1})	γ_i
A	DATA	124.0	1.2	1.8
A$'$	DATA	169.8	1.3	1.42
B	DALA	204.1	1.6	1.46
C	DATO	380.7	3.9	1.90
D	DALO	498.8	4.7	1.75
D$'$	DALO	567.2	3.7	1.21

acoustic (DATA) modes, while feature B is assigned to longitudinal acoustic (DALA) modes. On the other hand, the transverse optical branches give rise to a very broad band in the 1-PDOS, centered only slightly above 400 cm^{-1} (Fig. 2). Thus, we assign feature C to disorder-activated transverse optical (DATO) modes. With regard to the LO branch, the *ab initio* lattice-dynamical calculations yield a much narrower feature in the one-phonon DOS which is centered just below 600 cm^{-1} at 15 GPa. The pressure behavior of this feature resembles that of bands D and D$'$ observed experimentally. Bearing in mind the limitations of the *ab initio* calculations for the determination of LO frequencies, these two bands can be assigned to disorder-activated LO (DALO) modes.

The frequency of features A to D$'$, as obtained from the Raman spectra of sample C up to 20 GPa, is plotted with triangles in Fig. 6. Data obtained in the subsequent downstroke cycle at pressure values below the wurtzite-to-rocksalt transition pressure have also been included in the figure (see the next section for details). Table IV shows the resulting ω_{i0} and a_i values as obtained from a linear regression to the data of Fig. 6. In the case of bands A, A$'$, and B, relatively low a_i values are measured (1.2–1.6 cm^{-1} GPa^{-1}), which is a consequence of the acoustic nature of these bands. In the case of the optical features (C, D, and D$'$), larger a_i values are obtained (3.7–4.7 cm^{-1} GPa^{-1}). These values are consistently higher than those reported in Ref. 5, where a_i values below 3 cm^{-1} GPa^{-1} were measured. We believe that this difference is a consequence of the different pressure ranges investigated in both works, together with the expected reduced compressibility of the material with increasing pressure. In the case of Ref. 5, the wide pressure range investigated, up to 50 GPa, could have yielded underestimated linear pressure coefficients. Note that, in contrast, the a_i values measured in the present work are consistent with the DFT-LDA calculations for the zone-center TO and LO modes of rs-InN at 15 GPa (see Table III). Although the pressure behavior of the DATO and DALO bands is not expected to be exactly coincident with that of the zone-center optical modes, the consistency between the calculated values and the a_i values measured for features C, D, and D$'$ further suggests that underestimated a_i values were obtained in Ref. 5.

E. Rocksalt-to-wurtzite backtransformation

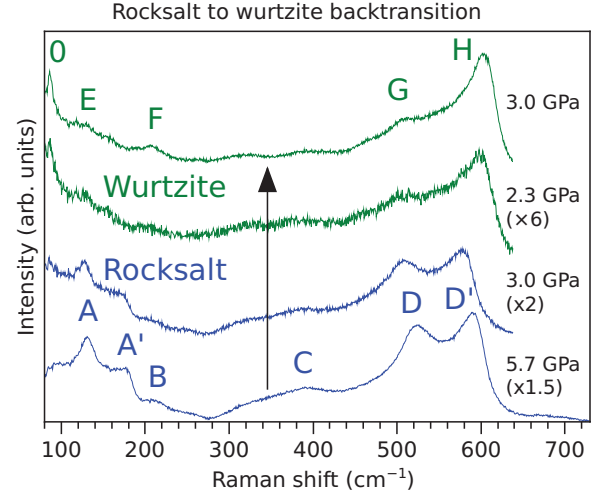Raman measurements in the downstroke cycle were also performed on sample C in order to investigate the

FIG. 12. (Color online) Raman spectra of rs-InN at 5.7 and 3.0 GPa and of w-InN at 2.3 GPa obtained during the down-stroke cycle, and of w-InN at 3.0 GPa after a subsequent up-stroke cycle.

backtransformation of the rocksalt phase to the wurtzite phase. Figure 12 shows Raman spectra obtained at 5.7, 3.0, and 2.3 GPa in the downstroke cycle and an additional spectrum (upper curve) obtained after increasing the pressure up to 3.0 GPa. The figure clearly shows that the rocksalt phase is metastable down to pressure values as low as 3.0 GPa. At lower pressures (2.3 GPa), the rocksalt-to-wurtzite backtransition is observed, and new features (labeled O, E, F, G, and H) appear in the Raman spectra. In particular, it should be noted that, for similar pressure values, feature H in the backtransited wurtzite phase is located at higher frequencies than feature D$'$ in the rocksalt phase (see also Fig. 6). Similarly, the relative intensity between features H and G is markedly different to that observed between bands D and D$'$ in rs-InN (see also the upper curve of Fig. 13 corresponding to backtransited w-InN at 9.8 GPa).

In Fig. 6 we have plotted the frequency position of all the features that show up in the Raman spectra of disordered w-InN as measured in the downstroke cycle and also during a subsequent upstroke cycle up to $\sim$10 GPa (open circles). As can be seen in the figure, the pressure behavior of features O, G, and H closely follows that of the E_{2l}, E_{2h}, and LO modes of crystalline w-InN, respectively. This is confirmed in Fig. 13, where we have plotted Raman spectra of backtransformed (disordered) w-InN at 0 and 9.8 GPa, together with the calculated 1-PDOS of w-InN at very similar pressure values (0 and 10 GPa, respectively). Similar spectra were observed after a pressure cycle of 20 GPa on InN samples[50] and also in highly disordered material subject to a high-dose ion-beam implantation process.[51] The observed bands can be attributed to first-order modes activated by disorder in poorly crystalline (amorphized) w-InN. As can be seen in Fig. 13, features G and H resemble the 1-PDOS curves at the corresponding frequency regions, which are mainly dominated by E_{2h} modes and LO modes, respectively. In turn, feature O is found to redshift with increasing hydrostatic pressure (see Fig. 13), as occurs in the case of the E_{2l} branch and also of TA modes from high-symmetry and high-wave-vector points of
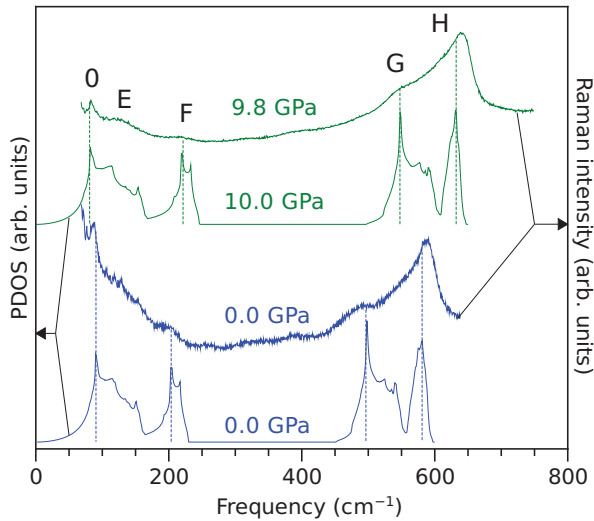
FIG. 13. (Color online) Raman spectra of poorly crystalline wurtzite InN after the rocksalt-to-wurtzite backtransition at ambient pressure and 9.8 GPa. For comparison, calculated one-phonon density of states (PDOS) curves at 0 and 10 GPa for w-InN are also shown.

the Brillouin zone in III–V semiconductors.[23,24] This band probably contains contributions from E_{2l} modes and also from TA modes along the entire Brillouin zone, which are activated by disorder in the backtransformed, poorly crystalline w-InN sample.

As can be seen in Fig. 13, the frequency and pressure behavior of features E and F is fairly reproduced in the calculated 1-PDOS curves. Following the data of this figure and also the phonon dispersion curves for w-InN as a function of pressure (see Fig. 1), it can be concluded that features E and F most likely arise from first-order DATA and DALA modes, respectively. Contributions to these bands from the E_{2l} and the (silent) B_{1l} branches cannot be ruled out.

The Raman-scattering results on backtransformed w-InN are similar to those obtained in AlN,[36] where the rocksalt-to-wurtzite backtransition pressure was found to occur around 1.3 GPa. In that work, taking into account that the wurtzite-to-rocksalt phase transition is completed only above 30 GPa, the return to the disordered wurtzite phase was tentatively attributed to an incomplete transition during the upstroke cycle arising from the nucleation of wurtzite microcrystals still present at the maximum applied pressures (25 GPa). Such an interpretation cannot be directly extrapolated to the present work, since the phase transition is expected to be complete at the maximum applied pressure ($\sim$20 GPa). In both cases, it would be highly interesting to investigate whether the backtransition occurs in samples that have been subject to very large hydrostatic pressures, i.e., to pressure values much higher than those corresponding to the wurtzite-to-rocksalt phase transition.

V. SUMMARY AND CONCLUSIONS

We have performed high-pressure Raman-scattering measurements on wurtzite InN (w-InN) epilayers grown by

plasma-assisted molecular beam epitaxy. The possible effect of residual strains on the measured pressure coefficients has been evaluated by studying different w-InN epilayers with different levels of built-in residual strain. The observed variation in the measured pressure coefficients for the E_{2h} and LO bands for all the samples investigated has been found to be lower than the typical error associated to this type of measurement. Thus, we conclude that the pressure coefficients extracted from the high-pressure Raman measurements are not affected by strain-related phenomena.

Pressure coefficients and the corresponding Grüneisen parameters have been measured for the zone-center E_{2l}, E_{2h}, A_1(TO), and E_1(TO) phonons of w-InN. The experimental data have been compared with theoretical results obtained from *ab initio* lattice-dynamical calculations as a function of hydrostatic pressure, with good agreement between the experimental and calculated pressure coefficients. The similar pressure coefficients obtained for the A_1(TO) and E_1(TO) modes suggest a small change in the anisotropy of w-InN with increasing pressure.

It has recently been shown that the LO modes of w-InN exhibit a strong wave-vector dependence that has been attributed to a selective resonance effect.[10] Given that the proposed double-resonance mechanism could affect the pressure behavior of the LO band, we have performed a calculation to evaluate the change of the pressure coefficient for the $q \neq 0$ LO modes as a function of the energy of the excitation radiation. The calculations reveal that the LO modes might display increased pressure coefficients for excitation energies close to the band gap of w-InN. High-pressure Raman experiments with different excitation wavelengths could be highly informative with regard to the double-resonance mechanism proposed in Ref. 10. In the case of visible or near-infrared radiation, the calculations suggest that no important pressure coefficient variations may be expected. The experimental pressure coefficients obtained for the A_1-E_1(LO) band with 632.8-nm excitation are in good agreement with the results of *ab initio* calculations for the A_1(LO) band, which confirms that the double-resonance mechanism does not significantly affect the pressure behavior of the LO band at these excitation conditions.

In w-InN samples with high levels of free electron concentration ($n_e = 1.6 \times 10^{19}$ cm^{-3}), the L^- coupled mode shows up in the Raman spectra. We have studied the pressure dependence of this mode, and we have used its frequency to evaluate the electron effective mass in w-InN as a function of pressure in the low-pressure regime. We have found a relative pressure coefficient for the electron effective mass [$\gamma_m = (d \ln m_e^*(p)/dp)_{p=0}$] equal to 0.031 ± 0.01 GPa^{-1}, in very good agreement with $\mathbf{k} \cdot \mathbf{p}$ theory. These results show the usefulness of Raman scattering to probe pressure-induced changes of the electronic structure of polar semiconductors.

For pressures above $\sim$13 GPa, peaks from rocksalt InN (rs-InN) show up in the Raman spectra. The spectra have been interpreted in terms of *ab initio* lattice-dynamical calculations as a function of pressure. We conclude that the features that appear in the Raman spectra of rs-InN can be assigned to disorder-activated first-order modes. Raman measurements in the downstroke cycle reveal that the rocksalt phase is

metastable down to pressure values as low as 3.0 GPa. Around 2.3 GPa, we find that the rocksalt-to-wurtzite backtransition occurs. The Raman spectrum of the backtransformed w-InN phase is dominated by disorder-activated first-order modes, as revealed by comparison of the Raman spectra with the calculated one-phonon density of states of w-InN.

*Corresponding author: jibanez@ictja.csic.es

[1] T. D. Veal, C. F. McConville, and W. J. Schaff (eds.), *Indium Nitride and Related Alloys* (CRC Press/Taylor Francis, Boca Raton, FL, 2010).

[2] J. Wu, J. Appl. Phys. **106**, 011101 (2009).

[3] T. Suski and W. Paul (eds.), *High Pressure in Semiconductor Physics I and II*, Semiconductors and Semimetals Vols. 54 and 55 (Academic Press, New York, 1998).

[4] C. Pinquier, F. Demangeot, J. Frandon, J. W. Pomeroy, M. Kuball, H. Hubel, N. W. A. van Uden, D. J. Dunstan, O. Briot, B. Maleyre, S. Ruffenach, and B. Gil, Phys. Rev. B **70**, 113202 (2004).

[5] C. Pinquier, F. Demangeot, J. Frandon, J. C. Chervin, A. Polian, B. Couzinet, P. Munsch, O. Briot, S. Ruffenach, B. Gil, and B. Maleyre, Phys. Rev. B **73**, 115211 (2006).

[6] L. D. Yao, S. D. Luo, X. Shen, S. J. You, L. X. Yang, S. J. Zhang, S. Jiang, Y. C. Li, J. Liu, K. Zhu, Y. L. Liu, W. Y. Zhou, L. C. Chen, C. Q. Jin, R. C. Yu, and S. S. Xie, J. Mater. Res. **25**, 2330 (2010).

[7] J. Ibáñez, F. J. Manjón, A. Segura, R. Oliva, R. Cuscó, R. Vilaplana, T. Yamaguchi, Y. Nanishi, and L. Artús, Appl. Phys. Lett. **99**, 011908 (2011).

[8] S. Uehara, T. Masamoto, A. Onodera, M. Ueno, O. Shimomura, and K. Takemura, J. Phys. Chem. Solids **58**, 2093 (1997).

[9] M.-Y. Duan, L. He, M. Xu, M.-Y. Xu, S. Xu, and K. K. Ostrikov, Phys. Rev. B **81**, 033102 (2010).

[10] V. Yu. Davydov, A. A. Klochikhin, A. N. Smirnov, I. Yu. Strashkova, A. S. Krylov, Hai Lu, W. J. Schaff, H.-M. Lee, Y.-L. Hong, and S. Gwo, Phys. Rev. B **80**, 081204(R) (2009).

[11] R. Cuscó, J. Ibáñez, E. Alarcón-Lladó, L. Artús, T. Yamaguchi, and Y. Nanishi, Phys. Rev. B **79**, 155210 (2009).

[12] S. Ernst, A. R. Goñi, K. Syassen, and M. Cardona, J. Phys. Chem. Sol. **56**, 567 (1995).

[13] S. Ernst, A. R. Goñi, K. Syassen, and M. Cardona, Phys. Rev. B **53**, 1287 (1996).

[14] Y. C. Lin, C. H. Chiu, W. C. Fan, C. H. Chia, S. L. Yang, D. S. Chuu, M. C. Lee, W. K. Chen, W. H. Chang, and W. C. Chou, J. Appl. Phys. **102**, 123510 (2007).

[15] ABINIT is a common project of the Université Catholique de Louvain, Corning Incorporated, and other contributors, http://www.abinit.org; X. Gonze, J.-M. Beuken, R. Caracas, F. Detraux, M. Fuchs, G.-M. Rignanese, L. Sindic, M. Verstraete, G. Zerah, F. Jollet *et al.*, Comput. Mater. Sci. **25**, 478 (2002).

[16] S. Goedecker, M. Teter, and J. Hütter, Phys. Rev. B **54**, 1703 (1996).

[17] N. Troullier and J. L. Martins, Phys. Rev. B **43**, 1993 (1991).

[18] M. F. Wu, S. Q. Zhou, A. Vantomme, Y. Huang, H. Wang, and H. Yang, J. Vac. Sci. Technol. A **24**, 275 (2006).

[19] M. Ueno, M. Yoshida, A. Onodera, O. Shimomura, and K. Takemura, Phys. Rev. B **49**, 14 (1994).

[20] J. Serrano, A. Bosak, M. Krisch, F. J. Manjón, A. H. Romero, N. Garro, X. Wang, A. Yoshikawa, and M. Kuball, Phys. Rev. Lett. **106**, 205501 (2011), and references therein.

[21] P. Giannozzi, S. de Gironcoli, P. Pavone, and S. Baroni, Phys. Rev. B **43**, 7231 (1991).

[22] X. Gonze and C. Lee, Phys. Rev. B **55**, 10355 (1997).

[23] B. A. Weinstein, Solid State Commun. **24**, 595 (1977).

[24] E. V. Yakovenko, M. Gauthier, and A. Polian, JETP **98**, 981 (2004).

[25] J. Ibáñez, A. Segura, B. García-Domene, R. Oliva, F. J. Manjón, T. Yamaguchi, Y. Nanishi, and L. Artús, Phys. Rev. B **86**, 035210 (2012).

[26] J. Serrano, A. H. Romero, F. J. Manjón, R. Lauck, M. Cardona, and A. Rubio, Phys. Rev. B **69**, 094306 (2004).

[27] R. Cuscó, J. Ibáñez, N. Domènech-Amador, L. Artús, J. Zúñiga-Pérez, and V. Muñoz-Sanjosé, J. Appl. Phys. **107**, 063519 (2010).

[28] R. Cuscó, E. Alarcón-Lladó, J. Ibáñez, T. Yamaguchi, Y. Nanishi, and L. Artús, J. Phys.: Condens. Matter **21**, 415801 (2009).

[29] R. Cuscó, J. Ibáñez, E. Alarcón-Lladó, L. Artús, T. Yamaguchi, and Y. Nanishi, Phys. Rev. B **80**, 155204 (2009).

[30] X. Wang, S.-B. Che, Y. Ishitani, and A. Yoshikawa, Appl. Phys. Lett. **89**, 171907 (2006).

[31] P. Perlin, C. Jauberthie-Carillon, J. P. Itie, A. San Miguel, I. Grzegory, and A. Polian, Phys. Rev. B **45**, 83 (1992).

[32] P. Perlin, T. Suski, J. W. Ager III, G. Conti, A. Polian, N. E. Christensen, I. Gorczyca, I. Grzegory, E. R. Weber, and E. E. Haller, Phys. Rev. B **60**, 1480 (1999).

[33] M. P. Halsall, P. Harmer, P. J. Parbrook, and S. J. Henley, Phys. Rev. B **69**, 235207 (2004).

[34] A. R. Goñi, H. Siegle, K. Syassen, C. Thomsen, and J.-M. Wagner, Phys. Rev. B **64**, 035205 (2001).

[35] G. H. Watson, W. B. Daniels, and C. S. Wang, J. Appl. Phys. **52**, 956 (1981).

[36] F. J. Manjón, D. Errandonea, A. H. Romero, N. Garro, J. Serrano, and M. Kuball, Phys. Rev. B **77**, 205204 (2008).

[37] N. Domènech-Amador, R. Cuscó, L. Artus, T. Stoica, and R. Calarco, Nanotechnology **23**, 085702 (2012).

[38] I. Gorczyca, J. Plesiewicz, L. Dmowski, T. Suski, N. E. Christensen, A. Svane, C. S. Gallinat, G. Koblmueller, and J. S. Speck, J. Appl. Phys. **104**, 013704 (2008).

[39] M. Cardona and G. Güntherodt, *Light Scattering in Solids IV*, Topics in Applied Physics (Springer-Verlag, Berlin, 1984), Vol. 54.

[40] L. Artús, R. Cuscó, J. Ibáñez, N. Blanco, and G. González-Díaz, Phys. Rev. B **60**, 5456 (1999).

[41] J. Ibáñez, R. Cuscó, and L. Artús, Phys. Status Solidi B **223**, 715 (2001).

[42] A. Kasic, M. Schubert, Y. Saito, Y. Nanishi, and G. Wagner, Phys. Rev. B **65**, 115206 (2002).

[43] F. Demangeot, C. Pinquier, J. Frandon, M. Gaio, O. Briot, B. Maleyre, S. Ruffenach, and B. Gil, Phys. Rev. B **71**, 104305 (2005).

[44] J. S. Thakur, D. Haddad, V. M. Naik, R. Naik, G. W. Auner, H. Lu, and W. J. Schaff, Phys. Rev. B **71**, 115203 (2005).

[45]T. Inushima, M. Higashiwaki, and T. Matsui, Phys. Rev. B **68**, 235204 (2003).

[46]A. Kasic, E. Valcheva, B. Monemar, H. Lu, and W. J. Schaff, Phys. Rev. B **70**, 115217 (2004).

[47]J. Wu, W. Walukiewicz, W. Shan, K. M. Yu, J. W. Ager, E. E. Haller, H. Lu, and W. J. Schaff, Phys. Rev. B **66**, 201403 (2002).

[48]J. G. Kim, Y. Kamei, N. Hasuike, H. Harima, K. Kisoda, K. Sasamoto, and A. Yamamoto, Phys. Satatus Solidi C **7**, 1887 (2010).

[49]N. E. Christensen and I. Gorczyca, Phys. Rev. B **50**, 4397 (1994).

[50]S. V. Ovsyannikov, V. V. Shchennikov, A. E. Karkin, A. Polian, O. Briot, S. Ruffenach, B. Gil, and M. Moret, Appl. Phys. Lett. **97**, 032105 (2010).

[51]V. Yu. Davydov, A. A. Klochikhin, M. B. Smirnov, V. V. Etsev, V. D. Petrikov, I. A. Abroyan, A. I. Titov, I. N. Goncharuk, A. N. Smirnov, V. V. Mamutin, S. V. Ivanov, and T. Inushima, Phys. Status Solidi B **216**, 779 (1999).